



FULL PAPER

Dichiral [4.4.3.0^{1,5}]tridecane copper(II) cluster derived from a tripodal ligand having unsymmetrical podands and the linker: Synthesis, structure, surface grafting and catalytic aspects

Hemant Singh¹ | Navneet Taya¹ | Jyoti Agarwal¹ | Raghubir Singh² | Varinder Kaur¹ ¹Department of Chemistry, Panjab University, Chandigarh, India²DAV College, Chandigarh, India**Correspondence**Raghubir Singh, DAV College, Sector 10, Chandigarh 160011, India.
Email: raghubirsingh@davchd.ac.in

Varinder Kaur, Department of Chemistry, Panjab University, Chandigarh 160014, India.

Email: var_ka04@pu.ac.in

Funding information

Science and Engineering Research Board, Grant/Award Number: EMR/2016/006530; DST-FIST, Grant/Award Number: SR/FST/college-335/2016; UGC-JRF, Grant/Award Number: 2061510021

Pseudo-atranes have a significant role in catalysis; however, obtaining chiral pseudo-atranes for covalent functionalization of heterogeneous catalytic surfaces is very challenging. Herein, synthesis of a chiral tripodal amine [N{CH(CH₂Ph)CH₂OH}{CH₂(4-Br-C₆H₃OH)}{CH₂(2-CHO-4-Me-C₆H₂OH)}] (1) and a dichiral [4.4.3.0^{1,5}]tridecane copper(II) cluster, that is, (Cu[N{CH(CH₂Ph)CH₂OH}{CH₂(4-Br-C₆H₃O)}{CH₂(2-CHO-4-Me-C₆H₂O)}])₂ (2) is described. The compounds are characterized by elemental analyses, Fourier transform infrared (FT-IR) spectroscopy, mass spectrometry and single-crystal X-ray crystallography (for 2). The compound 2 is the first example of chiral pseudo-copper(II)atrane in which three unsymmetrical arms (two phenolic and a chiral ethanolic arm) are fused via Cu-N transannular bond. The free -CHO group present in one of the tricyclic arms of the 2 is tested as a linker to load it on 3-aminopropyltriethoxysilane-functionalized magnetic nanosilica for catalytic applications. The loading of 2 on magnetic nanosilica through -CHO was confirmed by FT-IR spectroscopy, and the 2-loaded magnetic nanosilica (Fe₃O₄@SiO₂/2) was characterized by powder X-ray diffraction, vibrating sample magnetometry, scanning electron microscopy, energy-dispersive X-ray spectroscopy and elemental mapping. The Fe₃O₄@SiO₂/2 was found highly efficient, retrievable, eco-friendly and green catalyst for obtaining β-amino alcohols in excellent yields in an aqueous medium. Overall, present work is the first report on synthetic, structural and catalytic aspects of dichiral cluster of copper(II)atrane possessing unsymmetrical tricyclic arms.

KEYWORDS

bisphenolate, pseudo-atrane, functionalized magnetic silica, unsymmetrical tripod, epoxide ring-opening

1 | INTRODUCTION

The [4.4.3.0^{1,5}]tridecane metal cages are continuously achieving interest due to their fascinating structural attributes and relevance in catalysis.^[1–6] These are named as ‘pseudo-atranes’ due to their structural analogy with metallatranes. The pseudo-atranes with [4.4.3.0^{1,5}]tridecane cage differ from the atranes (having [3.3.3.0^{1,5}]undecane metal cages) in terms of the number or composition of the tricyclic ring atoms.^[7–11] The bulky and less flexible skeletons of [4.4.3.0^{1,5}]tridecane cages encapsulate the metal from one side making the other side available for catalytic reactions. For example, tripodal ligands with bisphenolate arms serve as best ancillary ligating frameworks in catalytic applications due to their structural rigidity. The most recent contribution of bisphenolate armed [4.4.3.0^{1,5}]tridecane metallatranes as reaction mediators includes copolymerization reactions of CO₂ and cyclohexene oxide, polymerization of methacrylate, hydrophosphination of alkenes, alkynes and heterocumulenes, ring-opening polymerization of L-lactic acid, o-carboxy anhydrides and L-lactide, epoxidation, sulfoxidation and catechol oxidation and cycloaddition of epoxides.^[12–24] The metal centres of metallatranes catalysts are widely distributed among various elements, that is, s-block (K), p-block (Al), d-block (Ti, Zr, Zn, Cr, V, Mo, W) and f-block elements (Y, Yb, Nd, La, Sm). Although bisphenolate atranes of Fe(III), Co(III), Cu(II), Si(IV) and Sn(IV) are known; however, their use in catalysis is rarely reported.^[1,25,26] The inexpensiveness, convenient synthetic protocols and broad spectrum of copper(II) complexes in catalysis^[27–29] inspired us to synthesize the copper(II)atrane complex and extend its application in the catalysis.

Therefore, a novel amine ligand N{CH(CH₂Ph)CH₂OH}{CH₂(4–Br–C₆H₃OH)}{CH₂(2–CHO–4–Me–C₆H₂OH)} (**1**) having an ethanolic and two distinct phenolate podands was synthesized. The ligand was designed to introduce chirality in the flexible ethanolic arm so that a chiral centre could be generated for its application in asymmetric catalysis. Besides, one of the phenolate arms of **1** was introduced with –CHO group so that the ligating skeleton or its complex could be grafted on the solid surface to obtain the heterogeneous catalyst. The tripodal amine **1** was used as a ligand to obtain symmetric dinuclear cluster of copper(II) pseudo-atrane **2** which has two chiral centres in each tricyclic unit. The copper(II) pseudo-atrane was successfully loaded on magnetic silica nanoparticles by Schiff base (SB) condensation reaction of free –CHO group (of the tricyclic cage) and amino-functionalized silica nanoparticles to obtain Fe₃O₄@SiO₂/2. The loading of **2** on Fe₃O₄@SiO₂ surface by the formation of

azomethinic bond was confirmed by Fourier transform infrared (FT-IR) spectroscopy and Fe₃O₄@SiO₂/2 was characterized by powder X-ray diffraction (PXRD), vibrating sample magnetometry (VSM), scanning electron microscopy (SEM), energy-dispersive X-ray spectroscopy (EDS) and elemental mapping.

In the past, some excellent reports are available on the usage of copper functionalized magnetic nanosilica for catalyzing organic reactions like asymmetric Henry reaction (by bis(oxazoline)copper(II) complex grafted magnetic mesoporous silica^[30]), synthesis of 3,4-dihydropyrimidin-2(1H)-ones (by magnetic mesoporous SBA-15^[31]), Beckmann rearrangement in poly(ethylene glycol) (by copper(II) complex supported magnetic nanoparticles^[32]), synthesis of pyrano[2,3-b]pyridine-3-carboxamide (by Schiff-base copper(II) complex grafted magnetic material^[33]), Suzuki reaction (by copper/ppm palladium nanoparticles^[34]), aerobic oxidation of alcohols (by copper complex-grafted magnetic graphene oxide^[35]), click reaction (magnetic copper-pectin composite^[36]) and oxidation reactions at room temperature (chitosan-dithiocarbamate magnetic nanocomposite).^[37] Besides, grafting of chiral copper complexes on nonmagnetic mesostructured silica surfaces is also reported which includes bis(oxazoline)copper(II) complex for kinetic resolution of hydrobenzoin, enantioselective cyclopropanation Cu(II)salen complex grafted for Henry reaction and amino indanol-based copper(II) complex for the asymmetric hetero-Diels-Alder reaction.^[38–41] This is the first report where a dichiral [4.4.3.0^{1,5}]tridecane cage of copper is directly loaded to the magnetic nanosilica and the fabricated material was tested for catalyzing the synthesis of β-amino alcohols (precursors of many biological active compound, synthetic products and unsaturated amino acids^[42–44]) in aqueous conditions. Although the chiral copper complexes yield optically active compounds in bulk amounts even when present in traces and catalyse, a wide range of enantioselective reactions (Diels-Alder reaction, enantioselective aziridination and cyclopropanation, hydrosilylation of ketones and asymmetric Friedel-Crafts alkylation)^[45–49] unfortunately, Fe₃O₄@SiO₂/2 did not yield enantioselective products in ring-opening of epoxides. However, it offered exceptional advantages and is better over some copper(II)-based catalysts reported in the past for the synthesis of β-amino alcohols. For instance, it is better in terms of high yields, heterogeneous catalytic surface (over homogeneous catalysts copper-indole derivative,^[50] copper(II) tetra-fluoroborate,^[51] copper(II) acetoacetate complex^[52] and in situ generated copper-allenyldiene intermediate^[53]), reusability and retrievability (over polymer-supported copper sulphate^[54] and copper coordination polymer

nanocrystals^[55]) and efficacy in the aqueous medium (copper doped spinal nano ferrites^[56]). Moreover, incorporation of the catalytic site on the surface of magnetic silica nanoparticles offers a clean, efficient and trouble-free separation with maximum recovery of the catalyst from the reaction mixture by using a magnet which is supported by previous literature.^[34–37]

2 | RESULTS AND DISCUSSION

2.1 | Synthetic aspects

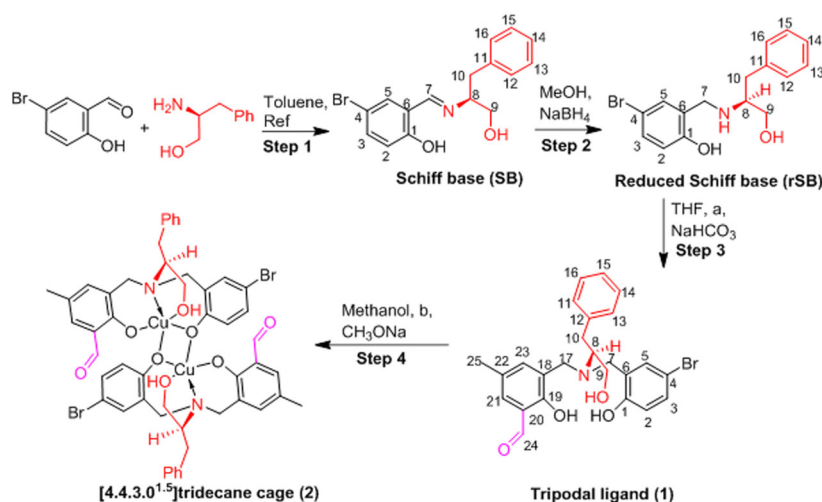
Synthesis of novel chiral tripodal ligand [N{CH (CH₂Ph)CH₂OH}{CH₂(4–Br–C₆H₃OH)}{CH₂(2–CHO–4–Me–C₆H₂OH)}] (**1**) was a three-step reaction. In the first step, equimolar amounts of L-phenylalaninol and 5-bromosalicylaldehyde were reacted to undergo a condensation reaction, which resulted in the formation of a chiral Schiff base (SB) with ONO donor system. In the second step, SB was reduced to generate secondary amine at the azomethinic position using NaBH₄ which afforded a dipodal-reduced Schiff base product (rSB) having a chiral ethanolic arm and a bisphenolate arm. It was further reacted with 3-(chloromethyl)-2-hydroxy-5-methylbenzaldehyde to introduce the third arm via a condensation reaction to obtain tertiary amine **1** (Scheme 1). The tripodal amine **1** consisted of a tetradentate NO₃ ligating framework with three distinct arms: a chiral ethanolic arm, the –Br substituted phenolic arm and the –CHO and –CH₃ substituted phenolic arm. The reaction of **1** with Cu (OAc)₂·2H₂O (in equimolar amount) in the presence of a base (sodium methoxide) afforded a green coloured complex. In the course of the reaction, sodium methoxide produced a tetradentate dianionic ligand by the deprotonation of

phenolic–OH arms (ethanolic proton remained intact) which coordinated with the copper ion to form a dinuclear cluster of dichiral [4.4.3.0^{1.5}]tridecane copper(II) cage, (Cu[N{CH (CH₂Ph)CH₂OH}{CH₂(4–Br–C₆H₃O)}{CH₂(2–CHO–4–Me–C₆H₂O)}])₂ (**2**).

2.2 | Spectroscopic aspects

The FT-IR spectrum of SB showed a strong band at 1633 and 3366 cm^{–1} due to –CH=N– and –OH stretching, respectively. In rSB, –OH vibrational band was observed as broadband in the region 2700–3000 cm^{–1} along with –NH stretching as a sharp single band at 3316 cm^{–1} suggesting the reduction of SB. The tripodal ligand **1** showed a vibrational band at 1651 cm^{–1} due to C=O vibration confirming the introduction of the phenolic arm with –CHO group (see Figures S1–S3).

The ¹H NMR spectrum of SB showed a singlet at 8.27 ppm for azomethinic proton (H⁷) along with double doublets at 2.82 and 3.00 ppm for diastereotopic protons H^{10a} and H^{10a'}. The phenolic –OH and ethanolic–OH resonances were observed as broad signals at 13.73 and 4.98 ppm, respectively. The signals for chiral proton H⁸ and diastereotopic H^{9b} were merged to give a multiplet in the range 3.47–3.55 ppm. In contrast, ¹H NMR spectrum of rSB consisted of four doublets of doublets (dd) centred at 3.30 ppm (for H^{9b}), 3.41 ppm (H^{9b'}), 3.82 ppm (for H^{7c}) and 3.87 ppm (H^{7c'}), respectively. The phenolic–OH, ethanolic–OH and secondary amine NH resonances were observed as a broad signal at 5.83 ppm. The ¹H NMR of tripodal ligand **1** exhibited a singlet at 9.83 ppm for aldehydic proton (H²⁴) and doublets of doublets each for diastereotopic protons H^{10a} and H^{10a'}, H^{9a} and H^{9b}, H^{7c} and H^{7c'} and H^{17d} and H^{17d'} showing AB spin system of diastereotopic protons. The signals of phenolic–OH and



SCHEME 1 A scheme for the synthesis of Schiff base (SB), reduced Schiff base (rSB), tripodal ligand **1** and [4.4.3.0^{1.5}]tridecane cluster **2** [where **a** = 3-(chloromethyl)-2-hydroxy-5-methylbenzaldehyde, **b** = Cu(OAc)₂·2H₂O] (the atoms are numbered to assign the NMR signals)

ethanolic—OH were not observed (see Figures S4–S6). The ^{13}C NMR spectra of SB, rSB and **1** showed characteristic signals at 160.3 (for C=N), 47.0 (for C—N) and 192.5 (for CHO), respectively (see Figures S7–S9). Further, electrospray-ionization mass spectra (ESI-MS) of SB, rSB and **1** exhibited molecular ion peaks at m/z 335.19, 336.23 and 484.01, respectively (see Figures S10–S12).

The copper atrane cage **2** consisted of vibrational bands at 1659 and 433 cm^{-1} due to $>\text{C}=\text{O}$ and Cu—N stretching, respectively. The Cu—O stretching vibrations generally lie between 345 and 305 cm^{-1} , therefore, were not observed in the FT-IR spectrum recorded in $4000\text{--}400\text{ cm}^{-1}$.^[57] The ESI-MS spectrum was consisted of a peak at m/z 1091.88 due to dinuclear cluster $(\text{Cu}[\text{N}\{\text{CH}(\text{CH}_2\text{Ph})\text{CH}_2\text{OH}\}\{\text{CH}_2(4\text{-Br-C}_6\text{H}_3\text{O})\}\{\text{CH}_2(2\text{-CHO-4-Me-C}_6\text{H}_2\text{O})\}])_2$ (see Figures S13–S15).

2.3 | Structural aspects

All the efforts to crystallize SB, rSB and **1** for single-crystal X-ray diffraction analysis were failed however **2** was crystallized from its ethanolic solution by slow evaporation. It was crystallized in an orthorhombic crystal system with $P2_12_12$ chiral space group. The structure of **2** consisted of a twofold symmetric dinuclear cluster formed by two $[4.4.3.0^{1.5}]$ tridecane cages. Each tricyclic cage $\text{Cu}[\text{N}\{\text{CH}(\text{CH}_2\text{Ph})\text{CH}_2\text{OH}\}\{\text{CH}_2(4\text{-Br-C}_6\text{H}_3\text{O})\}\{\text{CH}_2(2\text{-CHO-4-Me-C}_6\text{H}_2\text{O})\}]$ was constructed by two phenolate arms and an ethanolate arm which were fused to form a Cu—N transannular bond. The two $[4.4.3.0^{1.5}]$ tridecane cages were joined together via $\mu\text{-O}$ bridges formed by bromophenolate arms. This resulted in the formation of a rectangular core $\text{Cu}_2\text{-(}\mu\text{-OPh)}_2$ where two tricyclic cages were joined together (Figure 1a). Because all the three arms attached to nitrogen in the tripodal system were distinct, hence, **2** also acquired chirality with respect to nitrogen. The chirality of **2** was supported by

optical rotation value, that is, $[\alpha]_D = 234.76$. Therefore, complex **2** could be configured as S or R at the nitrogen atom. It was clear from the asymmetric unit (Figure 1b) that N and N1' acquired R and S configurations, respectively. So, the presence of two individual mononuclear entities with the opposite configuration in an asymmetric unit indicated the crystallization of **2** as a racemic mixture to tripodal nitrogen configuration (see Figure S16). Based on the crystal structure, overall configuration of chiral centres at N and C (i.e., N1, N1', C18 and C18') could be assigned as R, S, S and S (Figure 1b). The important structural parameters (i.e., bond angles and bond length), data collection parameters and structure refinement parameters for **2** are given in Tables 1 and 2.

The pentacoordinate Cu(II) exhibited distorted square pyramidal geometry with O1, O1', O3 and N1 at basal positions and O2 from the ethanolic arm at the apical position. The bond lengths of Cu—O bonds that lie in the basal plane are found to be Cu1—O1, 1.983(6) Å; Cu1—O1', 1.958(6) Å; Cu1—O3, 1.951(6) Å and Cu1—N1, 2.045(7) Å transannular. The bond length of apical bond, that is, Cu1—O2, 2.326(6) Å was found longest among all the basal bond lengths. The sum of all the basal angles is found to be 359.1° ($\angle\text{O1}^1\text{-Cu1-O1}$ ($75.2(3)^\circ$), $\angle\text{O1}^1\text{-Cu1-O3}$ ($94.5(3)^\circ$), $\angle\text{O1-Cu1-N1}$ ($92.6(3)^\circ$), $\angle\text{N1-Cu1-O3}$ ($96.8(3)^\circ$) and that for the angle formed with the apical O2 atom is 377.3° ($\angle\text{O2-Cu1-O1}^1$ ($103.7(2)^\circ$), $\angle\text{O2-Cu1-O1}$ ($97.1(2)^\circ$), $\angle\text{O2-Cu1-N1}$ ($80.4(3)^\circ$), $\angle\text{O2-Cu1-O3}$ ($96.1(3)^\circ$)). The efficient criterion for the 'GOODNESS' of the square pyramidal geometry is finding the difference of basal and apical angles from the ideal square pyramidal geometry, that is, $\Delta\Sigma(\theta)^\circ$ (basal) = $360 - \Sigma(\theta)_b^\circ$, where $\Sigma(\theta)_b^\circ$ is the sum of basal angles, and $\Delta\Sigma(\theta)^\circ$ (apical) = $360 - \Sigma(\theta)_a^\circ$, where $\Sigma(\theta)_a^\circ$ is the sum of apical angles. The goodness value of **2** around the copper for basal and apical atoms is 0.9° ($360^\circ - 359.1^\circ$) and 17.3° ($360^\circ - 377.3^\circ$), respectively (359.1° and 377.3° are the sums of basal and apical angles of

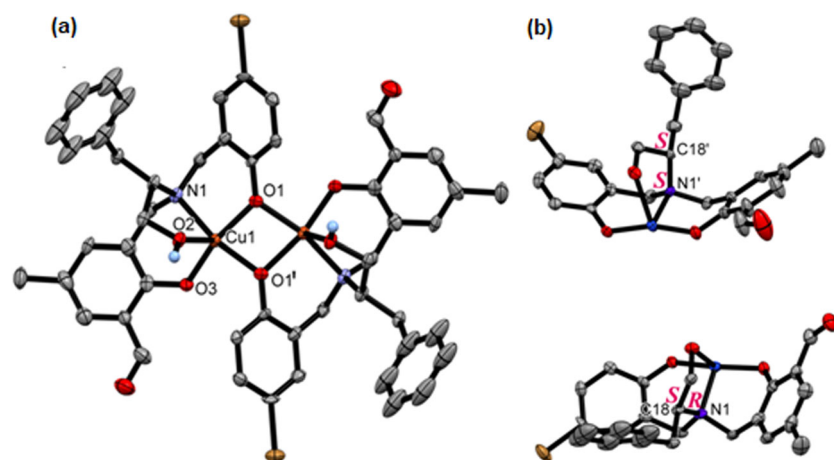


FIGURE 1 (a) ORTEP presentation of **2** with partial numbering scheme (thermal ellipsoids are drawn at 50% probability for nonhydrogen atoms and radius of hydrogen atoms were eliminated for clarity); (b) labelling of chiral centres to show stereospecific configuration

TABLE 1 Parameters of X-ray diffraction data collection and structure refinement of **2**

Parameters name	Parameter value	Parameters name	Parameter value
Empirical formula	C ₅₄ H ₆₆ Br ₂ Cu ₂ N ₂ O ₁₃	F(000)	2544
Formula weight	1237.98	Crystal size/mm ³	0.24 × 0.11 × 0.06
Temperature/K	99.99(10)	Radiation	Mo Kα (λ = 0.71073)
Crystal system	orthorhombic	2θ range for data collection/°	4.94 to 50.1
Space group	P2 ₁ 2 ₁ 2	Index ranges	−25 ≤ h ≤ 30, −20 ≤ k ≤ 20, −8 ≤ l ≤ 14
a/Å	25.3120(15)	Reflections collected	23183
b/Å	17.4464(8)	Independent reflections	9693 [R _{int} = 0.0517, R _{sigma} = 0.0811]
c/Å	12.3943(7)	Data/restraints/parameters	9693/84/611
α/°	90	Absorption correction	Multiscan
β/°	90	T _{min} /T _{max}	0.893/1.000
γ/°	90	Goodness-of-fit on F ²	1.041
Volume/Å ³	5473.4(5)	Final R indexes [I > =2σ (I)]	R ₁ = 0.0599, wR ₂ = 0.1412
Z	4	Final R indexes (all data)	R ₁ = 0.0774, wR ₂ = 0.1551
ρ _{calc} /cm ³	1.502	Largest diff. peak/hole/e Å ^{−3}	1.55/−1.12
μ/mm ^{−1}	2.301	Flack parameter	−0.005(7)

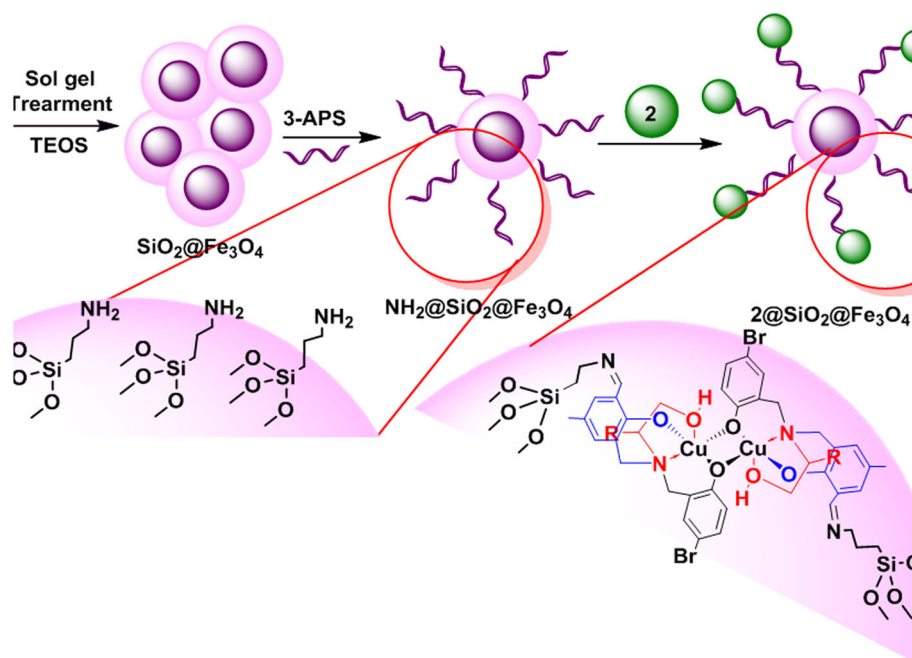
TABLE 2 Some important bonding parameters of **2**

Bond lengths of 2 (Å) at 100 K				Bond angles of 2 (°) at 100 K			
Br1—C4	1.893(4)	Br1'—C4'	1.882(4)	O11—Cu1—Cu11	40.18(18)	O1'—Cu1'—Cu1'1	39.09(18)
Cu1—Cu11	3.025(2)	Cu1'—Cu1'1	3.019(2)	O1—Cu1—Cu11	39.56(17)	O1'—Cu1'—Cu1'1	39.73(18)
Cu1—O1	1.983(6)	Cu1'—O1'1	1.967(6)	O11—Cu1—O1	75.2(3)	O1'—Cu1'—O1'1	76.3(3)
Cu1—O11	1.958(6)	Cu1'—O1'1	1.941(6)	O11—Cu1—O3	94.5(3)	O1'—Cu1'—O3'	92.1(2)
Cu1—O2	2.326(6)	Cu1'—O2'	1.897(7)	O1—Cu1—O3	164.9(3)	O1'1—Cu1'—O3'	100.7(2)
Cu1—O3	1.951(6)	Cu1'—O3'	2.359(6)	O1—Cu1—N1	92.6(3)	O1'1—Cu1'—N1'	170.1(3)
Cu1—N1	2.045(7)	Cu1'—N1'	2.045(8)	O11—Cu1—N1	167.5(3)	O1'—Cu1'—N1'	93.9(3)
O1—C1	1.358(7)	O1'—C1'	1.342(7)	O2—Cu1—Cu11	117.36(16)	O2'—Cu1'—Cu1'1	126.9(2)
O3—C8	1.353(8)	O2'—C8'	1.359(8)	O2—Cu1—O11	103.7(2)	O2'—Cu1'—O1'1	93.2(3)
O2—C17	1.442(11)	O3'—C17'	1.426(12)	O2—Cu1—O1	97.1(2)	O2'—Cu1'—O1'	165.3(3)
O4—C15	1.221(12)	O4'—C15'	1.230(15)	O2—Cu1—O3	96.1(3)	O2'—Cu1'—O3'	100.0(3)
N1—C7	1.519(12)	N1'—C7'	1.497(12)	O2—Cu1—N1	80.4(3)	O2'—Cu1'—N1'	96.2(3)
N1—C14	1.502(11)	N1'—C14'	1.509(11)	O3—Cu1—Cu11	126.50(19)	O3'—Cu1'—Cu1'1	108.84(15)
N1—C18	1.504(11)	N1'—C18'	1.510(11)	N1—Cu1—Cu11	127.4(2)	N1'—Cu1'—Cu1'1	131.1(2)
				N1—Cu1—O3	96.8(3)	N1'—Cu1'—O3'	81.0(3)

compound **2**, whereas 360° is that of the ideal geometry). The tau (τ) is another parameter (can be calculated as $\tau = (\beta - \alpha)/60$, where α and β are greatest basal angles and $\beta > \alpha$) is found to be 0.043 for this compound using the angles $\angle O1^1-Cu1-N1$, 167.5(3)° and $\angle O1-Cu1-O3$, 164.9(3)°, indicating its distorted square pyramidal geometry.^[58] The deviation from the ideal square pyramidal ($\tau = 0$) indicates distortion in the geometry.

2.4 | Surface functionalization aspects

The cluster of copper(II) pseudo-atrane was grafted directly on the surface of amino-functionalized magnetic nanosilica to fabricate **Fe₃O₄@SiO₂/2** (Scheme 2). For this, magnetic silica nanoparticles (synthesized via sol-gel method^[59,60]) were functionalized with 3-aminopropylsilatrane (via silanization^[59,60]) to



SCHEME 2 Fabrication of magnetic nanosilica $\text{Fe}_3\text{O}_4@SiO_2/2$ (where 3-APS is 3-aminopropylsilatrane)

introduce $-NH_2$ functionalities and the resulting material $\text{Fe}_3\text{O}_4@SiO_2/NH_2$ was reacted with 2. The $-NH_2$ groups present on the surface of $\text{Fe}_3\text{O}_4@SiO_2/NH_2$ were reacted with free $-CHO$ group on the ligating skeleton of 2 via Schiff base condensation yielding $\text{Fe}_3\text{O}_4@SiO_2/2$. This led to the covalent binding of 2 with the magnetic silica surface through azomethinic ($-N=CH-$) bond. To confirm the formation of azomethinic bond, FT-IR spectra of $\text{Fe}_3\text{O}_4@SiO_2/NH_2$ and $\text{Fe}_3\text{O}_4@SiO_2/2$ were compared. Both the materials showed some common vibrational bands at 590 cm^{-1} (for Fe–O stretching), 804 cm^{-1} (for Si–O–Si symmetric), 959 cm^{-1} (for Si–O symmetric stretching), 1090 cm^{-1} (for Si–O–Si asymmetric stretching) and some weak bands in the region

$2800\text{--}3000\text{ cm}^{-1}$ (for $>CH_2$ stretching and bending vibrations). However, FT-IR of $\text{Fe}_3\text{O}_4@SiO_2/2$ exhibited a vibrational band at 1633 cm^{-1} due to azomethinic bond and very weak bands in the range $1450\text{--}1670\text{ cm}^{-1}$ due to aromatic skeleton vibrations, which evidenced the immobilization of 2 on the surface of magnetic nanosilica via SB condensation (Figure 2a). The reaction of the carbonyl group with the 3-aminopropylsilyl group is very well known in literature.^[61–63]

The PXRD patterns of $\text{Fe}_3\text{O}_4@SiO_2/NH_2$ and $\text{Fe}_3\text{O}_4@SiO_2/2$ were found similar to patterns reported in the Joint Committee on Powder Diffraction Standards [JCPDS, ref. 19-629] with Bragg's diffraction peaks at 30.0° , 35.4° , 43.0° , 53.4° , 56.9° and 62.51° with reference

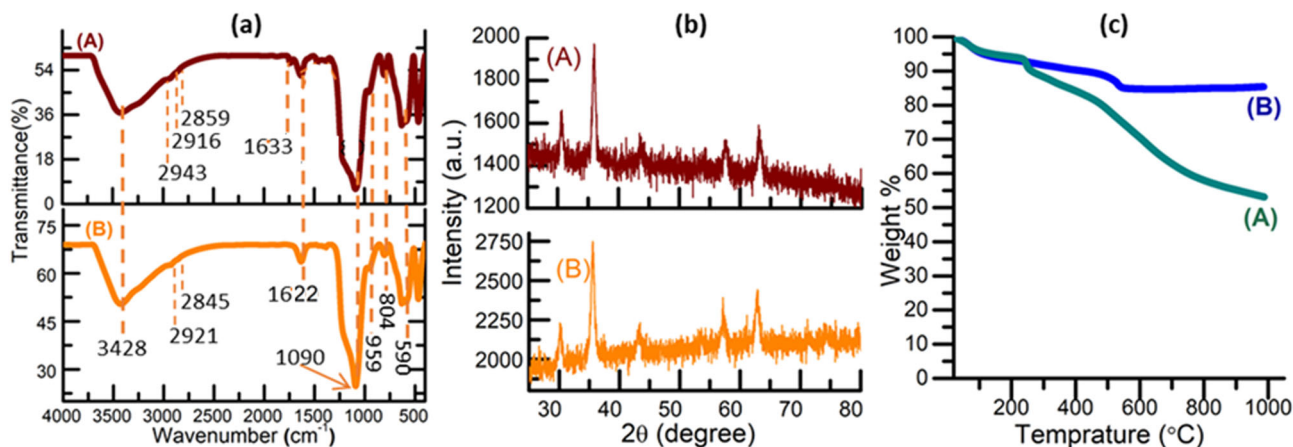


FIGURE 2 Comparison of characterization data of $\text{Fe}_3\text{O}_4@SiO_2/NH_2$ (B) and $\text{Fe}_3\text{O}_4@SiO_2/2$ (A); (a) Fourier transform infrared (FT-IR) spectra (b) powder X-ray diffraction (PXRD) curves (c) thermogravimetric analysis (TGA) plots

to (2 2 0), (3 1 1), (4 0 0), (4 2 2), (5 1 1) and (4 4 0) crystal planes of cubic spinel Fe_3O_4 , respectively (Figure 2b). The identical peaks in the X-ray diffraction patterns after modification of magnetic nanosilica indicated that the crystalline nature of the particles persisted even after the incorporation of silica and copper complex. The observed PXRD patterns are also supported by the literature reports.^[64] The average crystal size of nanosilica was obtained by the Debye Scherrer formula ($D_{hkl} = K\lambda/b \cos\theta$), where D is the size of the axis parallel to the (hkl) plane, K is a constant with a typical value of 0.89 for spherical particles, λ is the wavelength of radiation, b is full width at half maxima in radians and θ is the position of the diffraction maximum of the peak with the highest

intensity from the PXRD pattern. The crystallite size was found to be 14.7 and 14.4 nm for $\text{NH}_2\text{-Fe}_3\text{O}_4\text{@SiO}_2$ and $\text{Fe}_3\text{O}_4\text{@SiO}_2/2$, respectively. The values showed a slight reduction in crystallite size of $\text{Fe}_3\text{O}_4\text{@SiO}_2/2$ as compared with $\text{Fe}_3\text{O}_4\text{@SiO}_2/\text{NH}_2$ because the decrease in the average crystallinity of $\text{Fe}_3\text{O}_4\text{@SiO}_2/2$ due to coating of **2** resulted in the peak broadening. This proves the inverse relationship between crystallite size and full width at half maxima (b). Thermogravimetric (TG) curves of $\text{Fe}_3\text{O}_4\text{@SiO}_2/\text{NH}_2$ showed a decrease in mass up to 550°C because of the loss of physically adsorbed molecules like moisture, ethanol and alkyl chain; however, mass loss in $\text{Fe}_3\text{O}_4\text{@SiO}_2/2$ was continuous up to 1000°C indicating the loss of covalently bound

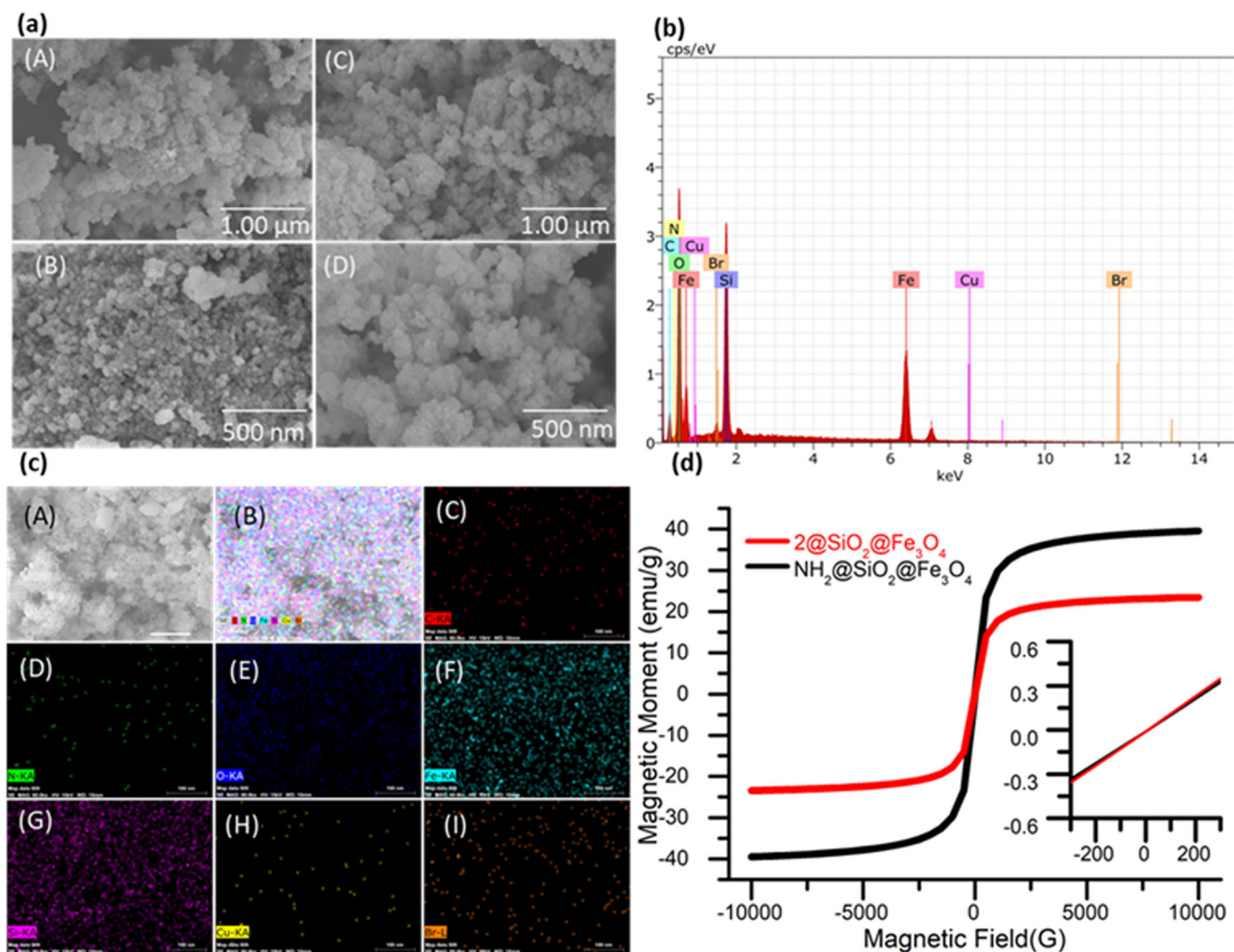


FIGURE 3 (a) Scanning electron microscopy (SEM) images of $\text{Fe}_3\text{O}_4\text{@SiO}_2/\text{NH}_2$ (A and B) and $\text{Fe}_3\text{O}_4\text{@SiO}_2/2$ (C and D); (b) energy-dispersive X-ray spectroscopy (EDS) of $\text{Fe}_3\text{O}_4\text{@SiO}_2/2$, (see Figure S17 EDS of $\text{Fe}_3\text{O}_4\text{@SiO}_2/\text{NH}_2$); (c) elemental mapping of $\text{Fe}_3\text{O}_4\text{@SiO}_2/2$ (A) area under observation, (B) elemental distribution of C, N, O, Fe, Si, Cu and Br, (C) distribution of carbon, (D) distribution of nitrogen, (E) distribution of oxygen, (F) distribution of iron, (G) distribution of silicon, (H) distribution of copper, (I) distribution of bromine (see Figure S18 for elemental mapping of $\text{Fe}_3\text{O}_4\text{@SiO}_2/\text{NH}_2$); (d) vibrating sample magnetometry (VSM) plot of $\text{Fe}_3\text{O}_4\text{@SiO}_2/\text{NH}_2$ and $\text{Fe}_3\text{O}_4\text{@SiO}_2/2$ and magnified view of the plot near the coercive field

alkyls and aryls. In the end, amounts left as oxides were 85.40 and 53.16% for $\text{Fe}_3\text{O}_4@\text{SiO}_2/\text{NH}_2$ and $\text{Fe}_3\text{O}_4@\text{SiO}_2/2$, respectively (Figure 2c).

The SEM images of $\text{Fe}_3\text{O}_4@\text{SiO}_2/\text{NH}_2$ and $\text{Fe}_3\text{O}_4@\text{SiO}_2/2$ displayed a roughly spherical morphology (Figure 3a). The surface roughening of $\text{Fe}_3\text{O}_4@\text{SiO}_2/2$ was apparent due to the deposition of silica shell around the magnetic core. Interestingly, no separate aggregates of silica were observed in the SEM images of the $\text{Fe}_3\text{O}_4@\text{SiO}_2/2$ which suggested that precipitation of silica was carried out only on the surface of the magnetic core.

The EDS of $\text{Fe}_3\text{O}_4@\text{SiO}_2/\text{NH}_2$ (see Figure S17) exhibited peaks of iron, oxygen, silicon, nitrogen and carbon verifying the coating of aminopropylsilicate on magnetic nanocores. In contrast, EDS of $\text{Fe}_3\text{O}_4@\text{SiO}_2/2$ consisted of additional peaks for copper and bromine confirming the grafting of **2** on the surface. The elemental mapping images of $\text{Fe}_3\text{O}_4@\text{SiO}_2/2$ clearly showed a uniform distribution of iron, oxygen, carbon, nitrogen, copper and bromine confirming the uniformity in the coating on the surface (Figure 3b). Further, elemental mapping images of $\text{Fe}_3\text{O}_4@\text{SiO}_2/2$ were compared with images of $\text{Fe}_3\text{O}_4@\text{SiO}_2/\text{NH}_2$. The elemental mapping images of $\text{Fe}_3\text{O}_4@\text{SiO}_2/\text{NH}_2$ clearly showed a uniform distribution of carbon, nitrogen, oxygen, silicon and iron (see Figure S18). Similarly, a uniform distribution of iron, oxygen, carbon, nitrogen, copper and bromine was observed in case of $\text{Fe}_3\text{O}_4@\text{SiO}_2/2$, thus confirming the incorporation of copper complex **2** on the surface of nanosilica (Figure 3c). The VSM studies were performed

to study the effect of grafted organic moieties on the magnetization behaviour of fabricated materials. The hysteresis curves revealed a reduction in saturation magnetization when $\text{Fe}_3\text{O}_4@\text{SiO}_2/\text{NH}_2$ (39.50 emu g^{-1}) was derivatized to $\text{Fe}_3\text{O}_4@\text{SiO}_2/2$ (23.40 emu g^{-1}) (Figure 3d). This phenomenon confirmed the dilution of magnetic centres due to loading of **2** on the surface of magnetic nanosilica. However, sufficient magnetization was observed for the separation of $\text{Fe}_3\text{O}_4@\text{SiO}_2/2$ from reaction media by applying a magnetic field. Moreover, $\text{Fe}_3\text{O}_4@\text{SiO}_2/2$ was found superparamagnetic because both magnetization, as well as demagnetization curves, passed through the origin showing negligible coercivity and remanence.

2.5 | Catalytic aspects

The catalytic activity of $\text{Fe}_3\text{O}_4@\text{SiO}_2/2$ was investigated for ring-opening reactions of epoxides (**3**) with substituted anilines (**4**). The effect of various important parameters such as catalyst loading, reaction time, temperature and solvent was optimized to achieve an optimum reaction condition. Initially, catalytic activity was investigated for the ring-opening reaction of cyclohexene oxide (**3a**) with aniline (**4a**). The reaction was performed in acetonitrile at different temperatures and with varying amounts of the catalyst which exhibited very low conversion of the reactants to product **5a** (ca. 22%–27% yields) even after a prolonged time of stirring (Table 3, entries 1–4).

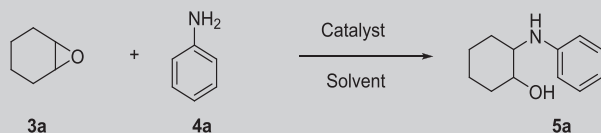


TABLE 3 Optimization of the reaction conditions

S. no.	Catalyst loading (mg)	Solvent	Temp (°C)	Time (h)	Yield ^a (%)
1.	20	ACN	50	48	27
2.	20	ACN	70	24	27
3.	30	ACN	rt	168	22
4.	100	ACN	70	48	27
5.	100	Toluene	110	24	22
6.	100	Water	100	22	84
7.	20	Water	80	22	98
8.	20	Water	100	24	82
9.	10	Water	80	22	94
10.	5	Water	80	22	84

^aIsolated yield.

Then, the same reaction was performed in toluene with 100 mg catalyst loading at reflux temperature, which yielded 22% of product **5a** (see Table 3, entry 5). Fortunately, when the reaction was performed in water using 100 mg catalyst loading at reflux temperature, 84% yield was obtained in 22 h (ca. 84%) (see Table 3, entry 6). Then, catalyst loading was reduced and next two reactions were carried out at 80°C and 100°C using 20 mg of

catalyst to afford the product **5a** in 98% and 82% yields, respectively (Table 3, entries 7 and 8). On the further decrease in catalyst loading to 10 and 5 mg at 80°C, a slight decrease in product yields to 94% and 84%, respectively, was observed (Table 3, entries 9 and 10).

Further, we investigated the substrate scope for the reaction. For that purpose, the reaction of cyclic and acyclic epoxides (**3a–c**) with various substituted aniline

TABLE 4 Substrate scope for the ring-opening reaction catalysed by $\text{Fe}_3\text{O}_4@\text{SiO}_2/2$.

R_1 R_2 + NH_2 R $\xrightarrow[\text{Water, 80 } ^\circ\text{C}]{\text{Catalyst (10mg)}}$ R_1 R_2 R
3a; $\text{R}_1, \text{R}_2 = -(\text{CH}_2)_4-$ **4a-d** **5a-d, 6a, 7a**
3b; $\text{R}_1, \text{R}_2 = -(\text{CH}_2)_3-$
3c; $\text{R}_1 = \text{H}, \text{R}_2 = \text{Ph}$

S. no.	Epoxide	Aniline		Product (s)		Time (h)	Yield (%)	TON
		R	No.	Structure	No.			
1.		H	4a		5a	22	94	503
2.		4-OMe	4b		5b	21	90	481
3.		4-Cl	4c		5c	24	91	487
4.		2-Cl	4d		5d	32	86	460
5.		H	4a		6a	18	92	492
6.		H	4a		7a	28	52	278

(4a–d) derivatives were performed at 80°C with 10 mg catalyst loading in water as a solvent. All reactions worked well, and excellent yields of the corresponding products were obtained. For example, in the reaction of 3a with 4-methoxyaniline 4b, the excellent yield for product 5b (90%) was obtained in 21 h (Table 4, entry 2). The reactions of chloro substituted anilines 4c and 4d took 24 and 32 h for completion to afford the products 5c and 5d in 91% and 86% yields, respectively (Table 4, entries 3 and 4). The lower yield and more reaction time for the 2-chloroaniline (4d) may be attributed to the steric hindrance caused by *ortho* substitution. When the reaction of cyclopentene oxide (3b) was performed with aniline (4a), product 6a was achieved in 92% yield (Table 4, entry 5). The reaction of styrene oxide (3c) with aniline (4a) provided only 52% yield of the product 7a in 28 h (Table 4, entry 6) (see Figures S19–S24 for ¹H NMR data).

The recyclability of the catalyst in aqueous medium was investigated for the reaction between cyclohexane (3a) and aniline (4a). The reaction was performed under optimized conditions as mentioned above. After the completion of the reaction, ethyl acetate was added, and the organic layer was extracted. This process was repeated for four times until the complete separation of organic compounds from the catalyst present in the aqueous layer was achieved. The organic layers were combined, dried over anhydrous sodium sulphate and evaporated to obtain a crude product, which was purified by using column chromatography. The catalyst was recovered from aqueous layer magnetically. Then, it was dried overnight at high temperature (above 100°C) in the oven and was used for subsequent cycles. The results obtained from the reusability of catalyst showed that Fe₃O₄@SiO₂/2 can be reused as an efficient catalyst for multiple runs but with slight loss of its catalytic activity (see Figure S25). The consistency in properties of the material was also supported by FT-IR and PXRD data of the material obtained after catalysis (see Figures S26 and S27).

The catalytic efficiency of the Fe₃O₄@SiO₂/2 was very high in water and provided the ring-opening products in excellent yields with very low catalyst loading. The quantitative loading of copper in the catalytic surface was obtained from EDS data of Fe₃O₄@SiO₂/2 which showed 1.19% (wt/wt) loading. It was used to calculate the turnover number (TON) using a formula reported in the literature.^[65] The tested catalytic system showed high catalytic efficiency with moderate to good TON (Table 4). When the reaction was performed in the presence of unsupported complex 2, only 5%–10% conversion of reactants was observed even after 48 h stirring at 80°C. However, loading of the complex 2 on the magnetic nanosilica improved the conversion percentage and reduced the

reaction time. Besides, usage of Fe₃O₄@SiO₂/2 was found beneficial over complex 2 because leaching of the catalyst was minimal due to covalent binding of the copper complex on the magnetic nanosilica. It was evidenced by the EDS data of recovered catalyst Fe₃O₄@SiO₂/2 (after catalytic reaction) which showed the presence of 1.10% (wt/wt) of copper in the material. Thus, Fe₃O₄@SiO₂/2 can be used as an eco-friendly and green catalyst for the synthesis of β-amino alcohols.

Although the stereoselective ring-opening of epoxides was not observed in the present case, however, it offered various advantages like excellent yields under mild reaction conditions, applicability in aqueous systems, easy isolation by using a magnet and reusability up to four cycles. Moreover, it is the first report where a copper(II)atrane complex is loaded on the solid surface and utilized for the catalytic purpose. The plausible cause for nonstereoselective results may be attributed either to the formation of the copper complex as a racemic mixture for chiral centre present at tripodal nitrogen atom or comparatively less loading of the complex on the magnetic nanosilica.

2.6 | Conclusion

A dinuclear cluster of dichiral copper(II)atrane can be derived from a tripodal ligand via step by step construction from L-phenylalanylol and 5-bromosalicylaldehyde. It consists of two [4.4.3.0¹⁻⁵]tridecane cages joined together through bridges formed by bromophenolate arms. Out of the remaining two arms of the tricyclic cage, ethanolic arm consists of a chiral centre and phenolate arm carries a free aldehydic (–CHO) functionality. This functionality can be used for the covalent grafting of copper(II) pseudo-atrane cluster on magnetic nanosilica Fe₃O₄@SiO₂/2. The 2 functionalized nanosilica can be utilized for catalyzing ring-opening of epoxides with aromatic amines which offers advantages of excellent yields even under mild reaction conditions and in the aqueous medium.

3 | EXPERIMENTAL

3.1 | Materials and methods

Syntheses of all the compounds were performed under a dry nitrogen atmosphere using Schlenk technique. Solvents toluene (Avra), tetrahydrofuran (THF) (Finar), ethanol (Merck) and methanol (Avra) were purchased commercially, dried and purified by standard procedures before use and stored under nitrogen atmosphere.

The chemicals such as 5-bromo-2-hydroxybenzaldehyde (Aldrich), 2-hydroxy-5-methylbenzaldehyde (TCI), copper(II)acetate dihydrate (Merck), ferric sulphate (Merck), ferrous sulphate heptahydrate (Merck), 3-aminopropyltriethoxysilane (Aldrich), sodium methoxide (Aldrich), sodium borohydride (Avra), sodium bicarbonate (Avra) and tetraethoxysilane (Aldrich) were used as such without any purification. The compounds L-phenylalaniol,^[66] 3-(chloromethyl)-2-hydroxy-5-methylbenzaldehyde^[67] and 3-aminopropyl-lisilatrane^[62,68] were synthesized using procedures reported in literature. The magnetic nano-cores (Fe_3O_4), magnetic nanosilica ($\text{Fe}_3\text{O}_4@\text{SiO}_2$) and aminopropyl functionalized magnetic nanosilica ($\text{Fe}_3\text{O}_4@\text{SiO}_2/\text{NH}_2$) were synthesized according to previously reported methods in literature^[51,52] (for detail procedure see Sections S2.1–S2.3).

3.2 | Physical measurements

The FT-IR spectra were recorded on Thermo Fischer Scientific NICOLET IS50-FT-IR for compounds and Perkin Elmer RX-I FT-IR spectrophotometer for silica nanoparticle materials. The NMR (^1H -NMR and ^{13}C -NMR) were recorded in CDCl_3 or DMSO-d_6 at room temperature by using Bruker Avance II FT NMR (AL 400 MHz) spectrometer. All chemical shifts (δ) were given in ppm relative to tetramethylsilane (TMS). The VG Analytical (70-S) spectrometer equipped with ESI source with capillary voltage 2500 V was used for ESI-MS measurements. Elemental analyses C, H and N were obtained by using a FLASH-2000 organic elemental analyser. The TG analyses of materials were done using an SDTQ-600 (TA instruments New Castle, DE). The magnetic studies of the materials were done using a VSM instrument Micro Sense EZ7. The PXRD data were obtained from PANalytical's X'Pert PRO diffractometer using $\text{Cu-K}\alpha$ radiation of wavelength 1.541 Å in 2θ range from 20° to 80° curves. The morphology was investigated by EDS and elemental mapping of materials was performed on Tescan Mira 3 field emission scanning electron microscopy (FESEM) instrument. All specific rotations ($[\alpha]_D$) were measured using Rudolph's AUTOPOL I Automatic polarimeter with single wavelength 589 nm (sodium lamp). The single-crystal X-ray diffraction data were collected on XtaLAB Mini (ROW) diffractometer using $\text{Mo-K}\alpha$ radiation ($\lambda = 0.71073$ Å). The crystal was kept at 99.99(10) K during data collection. Using Olex2, the structure was solved with the ShelXT structure solution program using intrinsic phasing and refined with the ShelXL using least squares minimization.^[69–71]

3.3 | Synthetic procedures

3.3.1 | Synthesis of SB

In a double-neck round bottom flask fitted with Dean Stark trap, a solution of 5-bromosalicylaldehyde (13.22 mmol, 2.66 g dissolved in 50 ml toluene) was added to L-phenylalaniol (13.22 mmol, 2.00 g dissolved in 50 ml toluene). The reaction mixture was heated to reflux for 5 h, and water produced during the reaction was removed azeotropically. The contents were cooled to room temperature, and toluene was removed under vacuum. The yellowish oily product was washed several times with fractions of hexane which yielded a yellow powder. Yield: 96% (12.66 mmol, 4.23 g), M.p.: $100\text{--}102^\circ\text{C}$; $[\alpha]_D = -195.7$; elemental analysis: Anal. Calculated for $\text{C}_{16}\text{H}_{16}\text{BrNO}_2$: C, 57.50; H, 4.83; N, 4.19; found: C, 57.76; H, 4.38; N, 4.09; % error: C, 0.26; H, 0.45; N, 0.01; FT-IR (cm^{-1}): 703 (C–Br), 1089, 1127 (C–O), 1367 ($>\text{CH}_2$, bending), 1476, 1571, 1601 (–C=C–, Aromatic), 1633 (–C=N), 2864, 2917, 3027 ($>\text{CH}_2$), 3366 (O–H); ^1H NMR (DMSO-d_6 , 400 MHz): δ (ppm) 2.82 (dd, 1H^{10a} , $^2,^3J = 13.5, 8.1$ Hz), 3.00 (dd, $1\text{H}^{10a'}$, $^2,^3J = 13.5, 4.0$ Hz), 3.47–3.55 (m, $2\text{H}^{8,9b}$), 3.66 (dd, $1\text{H}^{9b'}$, $^2J = 9.6$ Hz) 4.98 (b, 1H, OH), 6.85 (d, 1H^2 , $^3J = 8.8$ Hz), 7.14–7.27 (m, 5H^{12-16}), 7.43 (dd, 1H^3 , $^3,^4J = 8.8, 2.8$ Hz), 7.57 (d, 1H^5 , $^4J = 2.8$ Hz), 8.28 (s, 1H^7), 13.73 (b, 1H, Ph–OH); ^{13}C NMR (DMSO-d_6 , 100 MHz): δ (ppm) 38.2 (C^{10}), 64.1 (C^8), 72.0 (C^9), 108.8 (C^4), 119.0 (C^2), 120.2 (C^{14}), 126.1 (C^6), 128.2 ($\text{C}^{12,16}$), 129.3 ($\text{C}^{13,15}$), 133.4 (C^5), 134.6 (C^3), 138.4 (C^{11}), 160.3 (C^7), 164.2 (C^1); ESI-MS: m/z (relative abundance (%), fragment assigned): 334.04 [$100, \text{M} + \text{H}$]⁺, 336.04 [$99, \text{M} + 2 + \text{H}$]⁺.

3.3.2 | Synthesis of rSB

Sodium borohydride (14.95 mmol, 0.57 g) was added to 100 ml methanolic solution of SB (2.99 mmol, 1.00 g) under nitrogen atmosphere. The clear solution was stirred for 2 h at 50°C . The solvent was evaporated under vacuum and the residue was dissolved in chloroform (100 ml). The solution was shaken with distilled water (2×75 ml) to remove excessive sodium borohydride. The organic layer was separated, dried over anhydrous sodium sulphate and filtered. The solvent was removed under reduced pressure to afford rSB as a white solid. Step 2 yield: 94% (2.81 mmol, 0.95 g), Overall yield: 90% (2.68 mmol, 0.90 g); M.p.: $124\text{--}126^\circ\text{C}$; $[\alpha]_D = -18.60$; elemental analysis: Anal. Calculated for $\text{C}_{16}\text{H}_{16}\text{BrNO}_2$: C, 57.16; H, 5.40; N, 4.17; found: C, 57.56; H, 5.07; N, 4.24; % error: C, 0.40; H, 0.33; N, 0.07; FT-IR (cm^{-1}): 706 (C–Br), 1106, 1129 (C–O), 1343 ($>\text{CH}_2$, Bending),

1493, 1601(—C=C—, aromatic), 2858, 2916, 3031, 3058 (>CH₂), 3316 (>N—H), 3300–2700 (broad, O—H stretching, intramolecular hydrogen bonded); ¹H NMR (DMSO-d₆, 400 MHz): δ (ppm) 2.67–2.76 (m, 3H^{8,10a,10a'}), 3.30 (dd, 1H^{9b}, ^{2,3}J = 10.9, 5.0 Hz), 3.41 (dd, 1H^{9b'}, ^{2,3}J = 10.9, 4.0 Hz), 3.82 (d, 1H^{7c}, ²J = 14.5 Hz), 3.87 (d, 1H^{7c'}, ²J = 14.5 Hz), 5.83 (b, 3H, OH, Ph—OH, NH), 6.67 (d, 1H²), 7.19–7.30 (m, 7H^{3,5,12–16}); ¹³C NMR (DMSO-d₆, 100 MHz): δ (ppm) 37.0 (C¹⁰), 47.0 (C⁷), 59.9 (C⁸), 61.6 (C⁹), 109.5 (C⁴), 117.3 (C³), 125.8 (C²), 127.9 (C⁶), 128.1 (C^{12,16}), 129.2 (C^{13,15}), 130.1 (C¹⁴), 130.8 (C⁵), 139.4 (C¹¹), 156.4 (C¹); ESI-MS: *m/z* (relative abundance (%), fragment assigned): 336.06 [100, M + H]⁺, 338.05 [99, M + 2 + H]⁺.

3.3.3 | Tripodal ligand N{CH (CH₂Ph) CH₂OH}{CH₂(4—Br—C₆H₃OH)}{CH₂(2—CHO—4—Me—C₆H₂OH)} (1)

3-(chloromethyl)-2-hydroxy-5-methylbenzaldehyde (5.94 mmol, 1.10 g) and sodium bicarbonate (11.90 mmol, 1.00 g) were dissolved in THF (60 ml) in a two-necked flask fitted with a condenser and dropping funnel. Then, a solution of rSB (5.94 mmol, 2.00 g in 40 ml THF) was added to the mixture dropwise. The contents were heated to 50°C and stirred under nitrogen for 48 h. The progress of reaction was monitored with TLC. Then, the suspension (containing solid NaCl as by-product) was filtered and washed with THF. The solvent was removed under reduced pressure to afford a pale yellow solid. Step 3 yield: 94% (2.72 g, 5.64 mmol), Overall yield: 85% (2.45 g, 5.05 mmol); M.p.: 79°C–81°C; [α]_D = 5.35; elemental analysis: Anal. Calculated for C₁₆H₁₆BrNO₂: C, 61.99; H, 5.41; N, 2.89; found: C, 62.23; H, 5.58; N, 2.66; % error: C, 0.24; H, 0.17; N, 0.23; FT-IR (cm⁻¹): 698 (C—Br), 1030, 1112 (C—O), 1375 (>CH₂, bending), 1477, 1603 (—C=C—, Aromatic), 1651 (>C=O), 2846, 2918, 3027 (>CH₂) 3500–2700 (broad, O—H stretching, intramolecular hydrogen bonded); ¹H NMR (CDCl₃, 400 MHz): δ (ppm) 2.20 (s, 3H²⁵), 2.54 (dd, 1H^{10a}, ^{2,3}J = 13.2, 9.3 Hz), 3.07 (dd, 1H^{10a'}, ^{2,3}J = 13.2, 4.5 Hz), 3.10–3.16 (m, 1H⁸), 3.52 (d, 1H^{7c}, ²J = 13.0), 3.62 (dd, 1H^{9b}, ^{2,3}J = 12.2, 4.0 Hz), 3.66 (d, 1H^{17d}, ²J = 14.1), 3.81 (dd, 1H^{9b'}, ^{2,3}J = 12.1, 8.6 Hz), 4.04 (d, 1H^{17d'}, ²J = 14.1 Hz), 4.16 (d, 1H^{7c'}, ²J = 13.0 Hz), 6.57 (d, 1H², ³J = 8.5 Hz), 7.02 (d, 1H⁵, ⁴J = 2.4 Hz), 7.08 (s, 1H²³), 7.10 (s, 1H²¹), 7.16 (dd, 1H³, ^{3,4}J = 8.5, 2.4 Hz) 7.20–7.28 (m, 5H^{12–16}), 9.82 (s, 1H²⁴); ¹³C NMR (DMSO-d₆, 100 MHz): δ (ppm) 19.9 (C²⁵), 31.8 (C¹⁰), 48.3 (C⁷), 49.8 (C¹⁷), 59.5 (C⁹), 62.5 (C⁸), 109.9 (C⁴), 117.2 (C³), 121.5 (C²), 125.6 (C¹⁸), 125.9 (C⁶), 126.7

(C¹⁴), 127.7 (C²¹), 128.2 (C^{12,16,20}), 129.0 (C^{13,15}), 130.6 (C²²), 132.8 (C⁵), 137.3 (C¹¹), 140.0 (C²³), 155.4 (C¹), 158.1 (C¹⁹), 192.5 (C²⁴); ESI-MS *m/z* (relative abundance (%), fragment assigned): 484.01 [100, M + H]⁺, 486.02 [88, M + 2 + H], 336.35 [39, rSB + H]⁺, 300.35 [45, M—CH₂Ph(OH)(Br)]⁺.

3.3.4 | (Cu[N{CH (CH₂Ph)CH₂OH}{CH₂(4—Br—C₆H₃O)}{CH₂(2—CHO—4—Me—C₆H₂O)}])₂ (2)

The tripodal ligand **2** (1.03 mmol, 0.50 g) and sodium methoxide (3.09 mmol, 0.17 g) were dissolved in methanol (50 ml). The solution was stirred for 10 min at room temperature. Then, copper acetate dihydrate (1.00 mmol, 0.21 g) was added to the solution. The mixture was refluxed for 2 h, and the solvent was evaporated under vacuum. It resulted in a dark green residue which was dissolved in dichloromethane (30 ml) and washed with distilled water (2 × 30 ml). The organic layer was then separated, dried over anhydrous sodium sulphate and filtered, and the solvent was removed under reduced pressure to afford a dark green solid. The compound was recrystallized from ethanol by slow evaporation of solvent which resulted in crystals suitable for X-ray diffraction. Yield: 36% (0.20 g, 0.17 mmol, Step yield), Overall yield: 30% (0.17 g, 0.14 mol); M.p.: 236°C; [α]_D = 234.76; elemental analysis: Anal. Calculated for C₅₀H₄₈Br₂Cu₂N₂O₈: C, 55.00; H, 4.43; N, 2.57; found: C, 54.39; H, 4.75; N, 2.30; % error: C, 0.61; H, 0.32; N, 0.27; FT-IR (cm⁻¹): 706 (C—Br), 1568, 1614 (—C=C—, aromatic), 1659 (>C=O), 2864, 2974 (>CH₂); ESI-MS *m/z* (relative abundance [%], fragment assigned): 1091.88 [7, M + H]⁺, 1093.89 [4, M + 2 + H]⁺, 484.00 [100, 2 + H]⁺, 336.22 [22, M—CH₂Ph(OH)(CHO)(CH₃)]⁺, 300.35 [41, M—CH₂Ph(OH)(Br)]⁺.

3.3.5 | Grafting of **2** on magnetic silica nanoparticles (Fe₃O₄@SiO₂/2) and catalysis

A mixture of Fe₃O₄@SiO₂/NH₂ (1.00 g) and **2** (2.00 mmol, 2.38 g) in 100 ml ethanol was stirred at room temperature for 24 h. The resulting composite was removed magnetically, washed thoroughly with ethanol and dried. It was characterized by FT-IR, PXRD, SEM, EDS, VSM and TGA analysis, and the data were compared with Fe₃O₄@SiO₂/NH₂ to confirm the formation of Fe₃O₄@SiO₂/2. The fabricated material was used for catalyzing the synthesis of β-amino alcohols via ring-opening reactions (see Sections S2.4 and S2.5 for synthetic procedures and characterization details).

ASSOCIATED CONTENT

Supporting information—Procedure for the preparation of magnetite nanoparticles (Fe_3O_4), silica encapsulated magnetic nanocores ($\text{Fe}_3\text{O}_4@\text{SiO}_2$), amino-functionalized silica magnetic nanocores ($\text{Fe}_3\text{O}_4@\text{SiO}_2/\text{NH}_2$), ORTEP presentation of the asymmetric unit of **2**, thermogravimetric analysis of catalyst, energy dispersive X-ray spectrum of ($\text{Fe}_3\text{O}_4@\text{SiO}_2/\text{NH}_2$) elemental mapping data, catalytic recyclability data; FT-IR spectrum of the catalyst after the fourth cycle; PXRD data of catalyst after the fourth cycle; spectroscopic data (FT-IR, ^1H , ^{13}C , ^{119}Sn , and ESI-MS spectra) of SB, rSB, **1**, and **2**, General procedure for the ring-opening reactions; ^1H NMR data of products of catalysis experiments.

DATA AVAILABILITY STATEMENT

Experimental data and results are available in article supplementary material and crystallographic data is available in CCDC.

ACCESSION CODES

1951202 (**2**) contain the supplementary crystallographic data. The data can be obtained free of charge via www.ccdc.cam.ac.uk/data_request/cif, or by emailing data_request@ccdc.cam.ac.uk, or by contacting The Cambridge Crystallographic Data Centre, 12 Union Road, Cambridge CB2 1EZ, UK; fax: +44 1223 336033.

ACKNOWLEDGEMENTS

The authors are thankful to UGC, New Delhi for providing financial support under UGC-JRF scheme sr. no.: 2061510021, ref. no.: 21/06/2015(i)EU-V and DST, New Delhi (EMR/2016/006530) and DST-FIST (no. SR/FST/college-335/2016) for providing financial support.

AUTHOR CONTRIBUTIONS

Hemant Singh: Data curation; formal analysis; investigation; methodology. **NAVNEET TAYA**: Data curation; formal analysis; investigation; methodology. **Jyoti Agarwal**: Conceptualization; formal analysis; investigation; methodology. **Raghubir Singh**: Conceptualization; formal analysis; project administration; resources; supervision. **VARINDER KAUR**: Conceptualization; data curation; formal analysis; funding acquisition; investigation; methodology; project administration; resources; supervision; validation; visualization.

CONFLICTS OF INTEREST

There are no conflicts to declare.

ORCID

Hemant Singh  <https://orcid.org/0000-0001-5056-6131>
Navneet Taya  <https://orcid.org/0000-0002-0717-3145>

Jyoti Agarwal  <https://orcid.org/0000-0001-5516-7906>
Raghubir Singh  <https://orcid.org/0000-0003-1156-9174>
Varinder Kaur  <https://orcid.org/0000-0002-4585-0426>

REFERENCES

- [1] N. Srivastav, R. Mutneja, N. Singh, R. Singh, V. Kaur, J. Wagler, E. Kroke, *Eur. J. Inorg. Chem.* **2016**, 2016, 1730.
- [2] E. Safaei, T. Weyhermüller, E. Bothe, K. Wiegardt, P. Chaudhuri, *Eur. J. Inorg. Chem.* **2007**, 2007, 2334.
- [3] S. Groysman, I. Goldberg, M. Kol, E. Genizi, Z. Goldschmidt, *Organometallics* **2003**, 22, 3013.
- [4] T. Han, J.-F. Ma, G. Ping, Z. Jia, *Acta Crystallogr. Sect. E Struct. Reports Online* **2007**, 63, m2301.
- [5] A. K. Boudalis, R. E. Aston, S. J. Smith, R. E. Mirams, M. J. Riley, G. Schenk, A. G. Blackman, L. R. Hanton, L. R. Gahan, *Dalton Trans.* **2007**, 9226, 5132.
- [6] S. Padmanabhan, W. Wang, S. Katao, K. Nomura, *Macromol. Symp.* **2007**, 260, 133.
- [7] B. Glowacki, M. Lutter, W. Hiller, K. Jurkschat, *Inorg. Chem.* **2019**, 58, 4244.
- [8] A. Martinez, L. Guy, J. P. Dutasta, *J. Am. Chem. Soc.* **2010**, 132, 16733.
- [9] A. Martinez, V. Robert, H. Gornitzka, J. P. Dutasta, *Chem.–Eur. J.* **2010**, 16, 520.
- [10] A. Zschunke, A. Tzschach, K. Pöncke, *J. Organomet. Chem.* **1973**, 51, 197.
- [11] T. Zöllner, C. Dietz, L. Iovkova-Berends, O. Karsten, G. Bradtmöller, A. K. Wiegand, Y. Wang, V. Jouikov, K. Jurkschat, *Inorg. Chem.* **2012**, 51, 1041.
- [12] L. Hua, B. Li, C. Han, P. Gao, Y. Wang, D. Yuan, Y. Yao, *Inorg. Chem.* **2019**, 58, 8775.
- [13] K. Ni, V. Paniez-Grave, C. M. Kozak, *Organometallics* **2018**, 37, 2507.
- [14] R. Xu, L. Hua, X. Li, Y. Yao, X. Leng, Y. Chen, *Dalton Trans.* **2019**, 48, 10565.
- [15] D. L. Coward, B. R. M. Lake, R. Poli, M. P. Shaver, *Macromolecules* **2019**, 52, 3252.
- [16] Y. Zhang, X. Wang, Y. Wang, D. Yuan, Y. Yao, *Dalton Trans.* **2018**, 47, 9090.
- [17] Y. Zhang, L. Qu, Y. Wang, D. Yuan, Y. Yao, Q. Shen, *Inorg. Chem.* **2018**, 57, 139.
- [18] C. Yao, Y. Yang, S. Xu, H. Ma, *Dalton Trans.* **2017**, 46, 6087.
- [19] H. Ouyang, K. Nie, D. Yuan, Y. Yao, *Dalton Trans.* **2017**, 46, 15928.
- [20] Y.-L. Duan, J.-X. He, W. Wang, J.-J. Zhou, Y. Huang, Y. Yang, *Dalton Trans.* **2016**, 45, 10807.
- [21] A. Kronast, D. Reiter, P. T. Altenbuchner, S. I. Vagin, B. Rieger, *Macromolecules* **2016**, 49, 6260.
- [22] P. Salonen, A. Peuronen, A. Lehtonen, *Inorg. Chem. Commun.* **2017**, 86, 165.
- [23] P. Gao, Z. Zhao, L. Chen, D. Yuan, Y. Yao, *Organometallics* **2016**, 35, 1707.
- [24] J. A. Schachner, N. C. Mösch-Zanetti, A. Peuronen, A. Lehtonen, *Polyhedron* **2017**, 134, 73.
- [25] S. Indira, G. Vinoth, M. Bharathi, S. Bharathi, A. Kalilur Rahiman, K. Shanmuga Bharathi, *Inorganica Chim. Acta* **2019**, 495, 118988.
- [26] A. Rajput, A. Kumar, A. Sengupta, P. Tyagi, H. Arora, *New J. Chem.* **2018**, 42, 12621.

- [27] J. Finet, A. Fedorov, S. Combes, G. Boyer, *Curr. Org. Chem.* **2002**, *6*, 597.
- [28] J. S. Johnson, D. A. Evans, *Acc. Chem. Res.* **2000**, *33*, 325.
- [29] A. Sakakura, K. Ishihara, *Chem. Soc. Rev.* **2011**, *40*, 163.
- [30] J.-M. Lee, J. Kim, Y. Shin, C.-E. Yeom, J. E. Lee, T. Hyeon, B. Moon Kim, *Tetrahedron: Asymmetry* **2010**, *21*, 285.
- [31] J. Mondal, T. Sen, A. Bhaumik, *Dalton Trans.* **2012**, *41*, 6173.
- [32] M. Keyhaniyan, A. Shiri, H. Eshghi, *Appl. Organomet. Chem.* **2018**, *32*, 4344.
- [33] S. M.-G. Yek, D. Azarifar, M. Ghaemi, H. Keypour, M. Mahmoudabadi, *Appl. Organomet. Chem.* **2019**, *33*, 4918.
- [34] K. Lamei, H. Eshghi, M. Bakavoli, S. Rostamnia, *Appl. Organometal. Chem.* **2017**, *31*, 3743.
- [35] H. Alamgholiloo, S. Rostamnia, K. Zhang, T. H. Lee, Y. S. Lee, R. S. Varma, H. W. Jang, *ACS Omega* **2020**, *5*, 5182.
- [36] E. Doustkhah, M. Heidarzadeh, S. Rostamnia, A. Hassankhani, B. Kazemi, X. Liu, *Mater. Lett.* **2016**, *2018*, 139.
- [37] E. Doustkhah, S. Rostamnia, B. Gholipour, B. Zeynizadeh, A. Baghban, R. Luque, *Mol. Catal.* **2017**, *434*, 7.
- [38] L. Carneiro, A. R. Silva, M. A. O. Lourenço, A. Mayoral, I. Diaz, P. Ferreira, *Eur. J. Inorg. Chem.* **2016**, *2016*, 413.
- [39] F. Fakhfakh, L. Baraket, A. Ghorbel, J. M. Fraile, J. A. Mayoral, *React. Kinet., Mech. Catal.* **2015**, *116*, 119.
- [40] M. Halder, P. Bhanja, M. M. Islam, A. Bhaumik, S. M. Islam, *New J. Chem.* **2018**, *42*, 11896.
- [41] L. Li, X. Li, C. Fan, B. Huang, Y. Li, A. Zheng, Y. Sun, *React. Kinet., Mech. Catal.* **2016**, *117*, 715.
- [42] A. Sharma, J. Agarwal, R. K. Peddinti, *Org. Biomol. Chem.* **2017**, *15*, 1913.
- [43] J. Agarwal, R. K. Peddinti, *ChemistrySelect* **2019**, *4*, 7745.
- [44] J. Agarwal, D. Rani, in *Chapter 2-Ring-Opening Reactions in Water*, (Eds: R. B. Inamuddin, A. M. Asiri), Elsevier **2020** 31.
- [45] Y. Liu, Z. Li, G. Yuan, Q. Xia, C. Yuan, Y. Cui, *Inorg. Chem.* **2016**, *55*, 12500.
- [46] M. Teci, N. Lentz, E. Brenner, D. Matt, L. Toupet, *Dalton Trans.* **2015**, *44*, 13991.
- [47] M. Johannsen, K. A. Jørgensen, *J. Org. Chem.* **1995**, *60*, 5757.
- [48] S. Gao, J. R. Chen, X. Q. Hu, H. G. Cheng, L. Q. Lu, W. J. Xiao, *Adv. Synth. Catal.* **2013**, *355*, 3539.
- [49] M. I. D. Mardjan, S. Perie, J. L. Parrain, L. Commeiras, *Org. Biomol. Chem.* **2017**, *15*, 3304.
- [50] M. Kokubo, T. Naito, S. Kobayashi, *Tetrahedron* **2010**, *66*, 1111.
- [51] A. Kamal, R. Ramu, M. A. Azhar, G. B. R. Khanna, *Tetrahedron Lett.* **2005**, *46*, 2675.
- [52] M. L. Kantam, B. Neelima, C. V. Reddy, R. Chakravarti, *Ind. Eng. Chem. Res.* **2007**, *46*, 8614.
- [53] G. Hattori, A. Yoshida, Y. Miyake, Y. Nishibayashi, *J. Org. Chem.* **2009**, *74*, 7603.
- [54] V. R. Yarapathy, S. Mekala, B. V. Rao, S. Tammishetti, *Catal. Commun.* **2006**, *7*, 466.
- [55] K. Rodpun, N. T. Lucas, E. W. Tan, C. J. Meledandri, *Cryst. Growth des.* **2016**, *16*, 3940.
- [56] A. Sheoran, M. Dhiman, S. Bhukal, R. Malik, J. Agarwal, B. Chudasama, S. Singhal, *Mater. Chem. Phys.* **2019**, *222*, 207.
- [57] M. Gaye, O. Sarr, A. S. Sall, O. Diouf, S. Hadabere, *Bull. Chem. Soc. Ethiop.* **1997**, *11*, 111.
- [58] A. W. Addison, T. N. Rao, J. Reedijk, J. van Rijn, G. C. Verschoor, *Dalton Trans.* **1984**, 1349.
- [59] R. K. Sharma, S. Dutta, S. Sharma, *Dalton Trans.* **2015**, *44*, 1303.
- [60] R. Mutneja, R. Singh, V. Kaur, J. Wagler, S. Fels, E. Kroke, *New J. Chem.* **2016**, *40*, 1640.
- [61] R. Mutneja, R. Singh, V. Kaur, J. Wagler, E. Kroke, S. K. Kansal, *Dyes Pigm.* **2017**, *139*, 635.
- [62] P. Narula, R. Mutneja, R. Singh, V. Kaur, *Appl. Organomet. Chem.* **2016**, *30*, 852.
- [63] R. Singh, R. Mutneja, V. Kaur, J. Wagler, E. Kroke, *J. Organomet. Chem.* **2013**, *724*, 186.
- [64] J. H. Jang, H. B. Lim, *Microchem. J.* **2010**, *94*, 148.
- [65] S. Kozuch, J. M. L. Marti, *ACS Catal.* **2012**, *2*, 2787.
- [66] M. J. McKennon, A. I. Meyers, K. Drauz, M. Schwarm, *J. Org. Chem.* **1993**, *58*, 3568.
- [67] Q. Wang, C. Wilson, A. J. Blake, S. R. Collinson, P. A. Tasker, M. Schröder, *Tetrahedron Lett.* **2006**, *47*, 8983.
- [68] R. Singh, J. K. Puri, V. K. Chahal, R. P. Sharma, P. Venugopalan, *J. Organomet. Chem.* **2010**, *695*, 183.
- [69] O. V. Dolomanov, L. J. Bourhis, R. J. Gildea, J. A. K. Howard, H. Puschmann, *J. Appl. Crystallogr.* **2009**, *42*, 339.
- [70] G. M. Sheldrick, *Acta Crystallogr. Sect. A Found. Crystallogr.* **2015**, *71*, 3.
- [71] G. M. Sheldrick, *Acta Crystallogr. Sect. C Struct. Chem.* **2015**, *71*, 3.

SUPPORTING INFORMATION

Additional supporting information may be found online in the Supporting Information section at the end of this article.

How to cite this article: Singh H, Taya N, Agarwal J, Singh R, Kaur V. Dichiral [4.4.3.0^{1,5}] tridecane copper(II) cluster derived from a tripodal ligand having unsymmetrical podands and the linker: Synthesis, structure, surface grafting and catalytic aspects. *Appl Organomet Chem.* 2020; e6075. <https://doi.org/10.1002/aoc.6075>